REPORT DOCUMENTATION PAGE

AFRL-SR-AR-TR-09-0249

1. REPORT DATE *(DD-MM-YYYY)*	2. REPORT TYPE	3. DATES COVERED *(From - To)*
27-05-2009	Final Report	March 31, 2007 – March 31, 2009

4. TITLE AND SUBTITLE "Predicting Flare Properties Using the Minimum Current Corona Model"

5a. CONTRACT NUMBER
FA9550-06-C-0019

5b. GRANT NUMBER

5c. PROGRAM ELEMENT NUMBER

6. AUTHOR(S)
Graham Barnes

5d. PROJECT NUMBER

5e. TASK NUMBER

5f. WORK UNIT NUMBER

7. PERFORMING ORGANIZATION NAME(S) AND ADDRESS(ES)

NorthWest Research Associates
4118 148th Ave. NE
PO Box 3027
Bellevue, WA 98009-3027

8. PERFORMING ORGANIZATION REPORT NUMBER
AFOSR C322P Final Report

9. SPONSORING / MONITORING AGENCY NAME(S) AND ADDRESS(ES)
Dr. Kent Miller
Air Force Office of Scientific Research
875 N. Randolph St. Suite 325, RM 3112
Arlington, VA 22203

10. SPONSOR/MONITOR'S ACRONYM(S)
AFOSR

11. SPONSOR/MONITOR'S REPORT NUMBER(S)

12. DISTRIBUTION / AVAILABILITY STATEMENT

13. SUPPLEMENTARY NOTES

14. ABSTRACT

The objective of our original proposal was to use the Minimum Current Corona (MCC) model to determine where strong currents are likely to develop above an active region, and compare the locations with observed flare signatures. If there is a good correspondence, we can also estimate the energy available for the flare from the current sheet in question. In the MCC model, the magnetic field in the corona is represented by the field due to a collection of point sources on the boundary: a Magnetic Charge Topology (MCT) model. Evolving these sources consistent with the evolution of the boundary causes currents to begin flowing in the corona. The minimum energy state occurs when currents flow only along separator field lines: topologically significant field lines which connect magnetic null points. In the absence of reconnection, the magnitudes of these currents can be estimated, along with the energy stored by each.

15. SUBJECT TERMS
Magnetic Charge Topology, Magnetic Helicity, Coronal Mass Ejections

16. SECURITY CLASSIFICATION OF: NONE			17. LIMITATION OF ABSTRACT	18. NUMBER OF PAGES	19a. NAME OF RESPONSIBLE PERSON
a. REPORT	b. ABSTRACT	c. THIS PAGE		13	David C. Fritts
					19b. TELEPHONE NUMBER *(include area code)* 303-415-9701

DEFENSE TECHNICAL INFORMATION CENTER

Information for the Defense Community

DTIC® has determined on 8/12/2009 that this Technical Document has the Distribution Statement checked below. The current distribution for this document can be found in the DTIC® Technical Report Database.

☒ **DISTRIBUTION STATEMENT A.** Approved for public release; distribution is unlimited.

☐ **© COPYRIGHTED**; U.S. Government or Federal Rights License. All other rights and uses except those permitted by copyright law are reserved by the copyright owner.

☐ **DISTRIBUTION STATEMENT B.** Distribution authorized to U.S. Government agencies only (fill in reason) (date of determination). Other requests for this document shall be referred to (insert controlling DoD office)

☐ **DISTRIBUTION STATEMENT C.** Distribution authorized to U.S. Government Agencies and their contractors (fill in reason) (date of determination). Other requests for this document shall be referred to (insert controlling DoD office)

☐ **DISTRIBUTION STATEMENT D.** Distribution authorized to the Department of Defense and U.S. DoD contractors only (fill in reason) (date of determination). Other requests shall be referred to (insert controlling DoD office).

☐ **DISTRIBUTION STATEMENT E.** Distribution authorized to DoD Components only (fill in reason) (date of determination). Other requests shall be referred to (insert controlling DoD office).

☐ **DISTRIBUTION STATEMENT F.** Further dissemination only as directed by (inserting controlling DoD office) (date of determination) or higher DoD authority.

Distribution Statement F is also used when a document does not contain a distribution statement and no distribution statement can be determined.

☐ **DISTRIBUTION STATEMENT X.** Distribution authorized to U.S. Government Agencies and private individuals or enterprises eligible to obtain export-controlled technical data in accordance with DoDD 5230.25; (date of determination). DoD Controlling Office is (insert controlling DoD office).

Final Report: AFOSR Contract FA9550-06-C-0019
Predicting Flare Properties Using the Minimum Current Corona Model

Principal Investigator: Graham Barnes
Institution: NorthWest Research Associates, 4118 148th Ave NE Redmond, WA 98052

Research Objectives:

The objective of our original proposal was to use the Minimum Current Corona (MCC) model to determine where strong currents are likely to develop above an active region, and compare the locations with observed flare signatures. If there is a good correspondence, we can also estimate the energy available for the flare from the current sheet in question. In the MCC model, the magnetic field in the corona is represented by the field due to a collection of point sources on the boundary: a Magnetic Charge Topology (MCT) model. Evolving these sources consistent with the evolution of the boundary causes currents to begin flowing in the corona. The minimum energy state occurs when currents flow only along separator field lines: topologically significant field lines which connect magnetic null points. In the absence of reconnection, the magnitudes of these currents can be estimated, along with the energy stored by each.

The objectives of the research were broadened to include an analysis of the injection of magnetic helicity into the solar corona. In brief, reconnection is likely to play a crucial role in the initiation or release of energy in solar flares, while helicity may provide insight into the mechanism responsible for Coronal Mass Ejections. We have used the partitioning needed to implement the MCC model to understand the way in which helicity is injected into the solar corona.

Our effort was also extended to justify the use of the MCC model. In particular, the scientific community has expressed skepticism that the MCT potential field is a good representation of the actual potential field, and a recent letter by Georgoulis & Rust (2007) suggested that a good parameter for forecasting major flares could be derived from simply the MCT connectivity at a given time. Thus we have spent time addressing both of these concerns.

Work Carried Out:

Instead of solving the full-blown magnetohydrodynamic (MHD) equations, the MCC models the coronal magnetic field with a collection of point sources on the boundary. In this case, the topology becomes particularly simple: with a few special exceptions, field lines begin and end on sources. One of the important exceptions is separator field lines, which begin and end on magnetic null points, and encircle bundles of flux connecting pairs of sources. The locations and magnitudes of the points sources (magnetic charges) are determined by partitioning the boundary field into flux concentrations; each partition is represented by a single point source. The potential field due to the collection of point sources, and thus the amount of flux connecting each pair of sources, is calculated at two times. The changes in the potential field connectivity are canceled by introducing currents along separators, and the free energy introduced is computed from these separator currents. The advantages to the model are that it shows *where* the energy is stored and how much can be liberated by a single reconnection event, and that it calculates the free energy directly, rather than taking the difference between

the total energy and the potential energy. A disadvantage is that the model must start from a potential field configuration, and thus can only track the *evolution* of the energy.

We have applied the MCC model to multiple time series of vector magnetograms from the Imaging Vector Magnetograph (IVM). The evolution of the free magnetic energy was tracked, and the location of the greatest energy storage was compared to the location of brightening in MCCD images. In addition, the MCC model was applied to the much longer time series of line of sight magnetograms available from the Michelson Doppler Imager (MDI) on board the SOHO space craft. The use of these longer time series required the development of a new partitioning algorithm. The validity of the partitioning was confirmed by comparing the source velocities to velocities determined using Local Correlation Tracking.

The new partitioning algorithm allowed us to decompose the magnetic helicity injected into the corona into a spin component and a braiding component. The former is likely to arise from the twist of sub-photospheric flux tubes, while the latter results from motion of flux tubes about one another. The partitioning algorithm was run for a number of time series of MDI data, and used to decompose the helicity injection. The relative importance of spin versus braiding helicity was determined.

Coronal magnetic field can be characterized by the way its field lines interconnect regions of positive and negative photospheric flux: its connectivity. Connectivity can be quantified as the net flux connecting pairs of opposing regions. It is rapid changes in this connectivity that are believed to release stored magnetic energy in the form of solar flares. We have performed a detailed comparison of the magnetic field connectivity for potential fields derived from both an MCT model, and from using the observed magnetic field on the whole boundary. In addition, we considered one further difference in the boundary: the field was either contained within conducting walls on four sides, or was allowed to expand to fill the half-space above the boundary. By doing this, we have been able to determine the limitations of determining the connectivity in an MCT model resulting from reducing the lower boundary to a collection of point sources, and thus have established the validity of this approximation in the MCC model.

Recent work by Georgoulis & Rust (2007) suggested that a parameter constructed from the connectivity of an MCT model is "an efficient flare-forecasting criterion". If it were indeed the case that a robust flare forecasting parameter could be constructed using only the connectivity in an MCT model at one time, then there would be less incentive to consider the MCC model. Thus we have replicated the approach of Georgoulis & Rust (2007) for our own data base of magnetic field observations, and compared the performance of their parameter to ones previously investigated.

Results Obtained:

Spatial Distribution and Evolution of the Free Energy

We have applied the MCC model to time series of vector magnetograms from the Imaging Vector Magnetograph (IVM) for several active regions which produced large flares. The results of the analysis for a sample active region (NOAA AR 10030) are shown in Figure 1. On the left, the partitioning of the magnetogram is shown, along with the locations of sources, nulls, spines and fan traces. Of particular interest is the coronal magnetic null at approximately (0,265) in the image.

To investigate the location, timing, and dynamics of chromospheric and photospheric emission associated with solar flares, we used data from the Mees CCD Imaging Spectrograph (MCCD). The MCCD routinely obtained Hα spectra with extremely high-cadence scans across

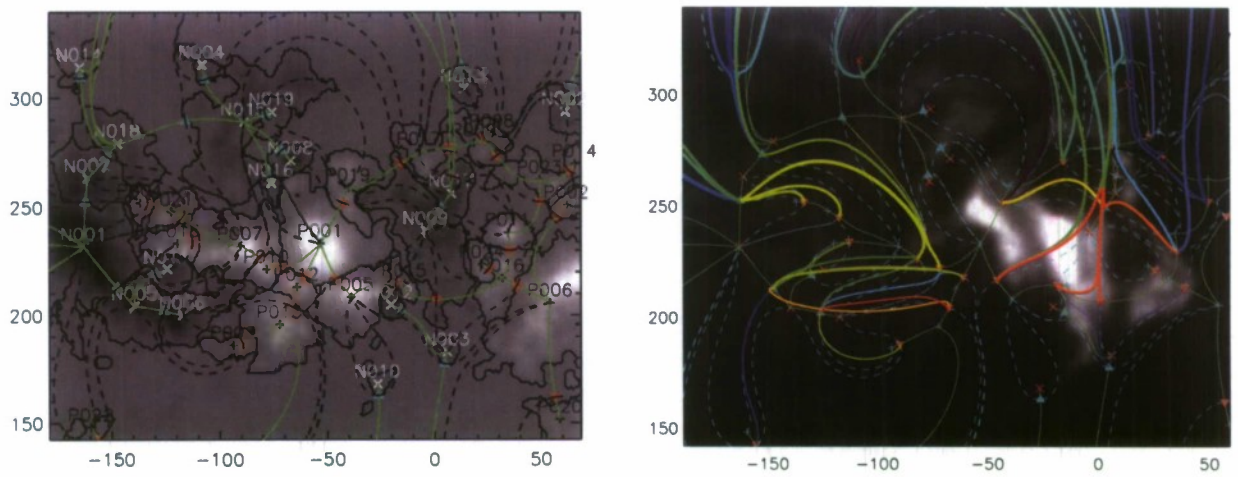

Figure 1: MCC analysis of NOAA AR 10030. **Left:** The vertical component of the magnetic field (greyscale) plus the partitioning (lines), locations of sources (plus and cross), nulls (triangles, blue for A-type and red for B-type, purple for coronal), spines (green lines), and fan traces (dashed lines). **Right:** An MCCD image of the thermal response in the chromosphere from Hα line-center images of the the flare ribbons which developed roughly 10 minutes after the peak soft X-ray flux, with the same sources, nulls, spines and fan traces. In addition, separator field lines are shown, with the color of each separator determined by the current along that separator, with red being the most energetic. Although the time series used is too short to encapsulated the full build up of energy, it is encouraging that some of the most energetic separators are in the vicinity of the brightest part of the MCCD image. Further, the brightening all occurs close to or within the separatrix surface of the coronal null point, indicating the possible importance of such topological features. This flare occurred in conjunction with a Coronal Mass Ejection (CME), so the presence of the coronal null point is consistent with the magnetic breakout model for CME initiation.

---

a target active region. The target for the MCCD was usually coordinated with that of the IVM, making a powerful data set of photospheric magnetic field evolution and chromospheric thermal response and dynamics during solar energetic events. On the right of Figure 1, an Hα line center image from the MCCD of the flare is shown, with the same sources, nulls, spines and fan traces. In addition, separator field lines are shown, with the color of each separator determined by the current resulting from the MCC model applied to a time series of approximately one hour duration. Although the exact location does not match, it is encouraging to note that several of the most energetic separators are in the vicinity of the brightest part of the MCCD image. In fact, the chromospheric brightening occurs primarily within the separatrix surface of the coronal null point. This flare occurred in conjunction with a Coronal Mass Ejection (CME), so the presence of the coronal null point is consistent with the magnetic breakout model for CME initiation.

The free energy estimate for this active region is much smaller than the energy typically released by a large flare. To further investigate the build up of energy, we have applied the MCC model to NOAA AR 8210 during the time leading up to the M1.2 flare on 1998 May 1. In particular, we used both an approximately five hour time series of IVM vector magnetogram data, and an approximately one day time series of MDI line of sight magnetogram data. In

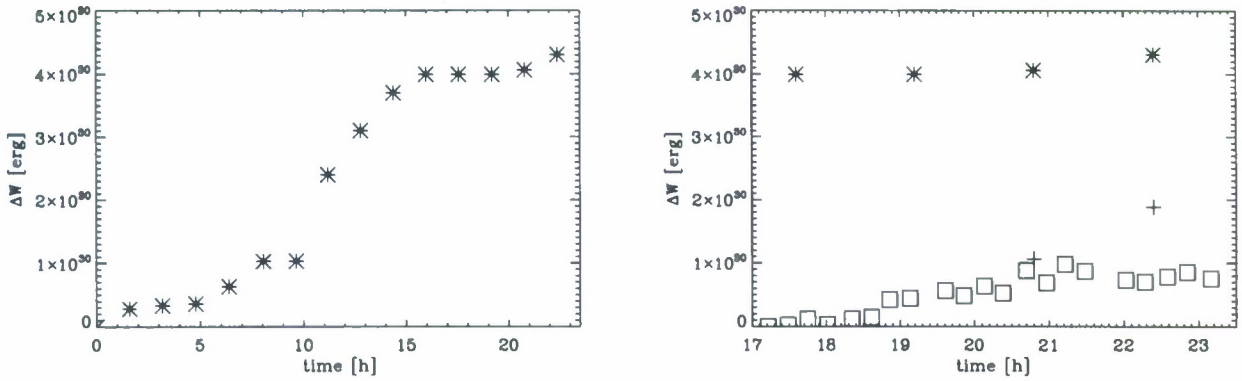

Figure 2: The magnetic free energy from the MCC model for NOAA AR 8210. **Left:** The entire time interval of MDI data considered, indicating that the energy builds up on a timescale of a day or longer. **Right:** Comparison of the energy derived from the IVM time series (squares) to the MDI time series, initiated at the same time as the IVM time series (pluses) and initiated approximately 17 hr earlier (asterisk). When initiated at the same time, the resulting energies are very similar, indicating that using the line of sight component of the field rather than the vertical component does not have a large effect over a short time interval, but may diverge for longer times.

---

both cases, the currents along separators was computed, and the free energy build up inferred. Figure 2 shows the result for the both the full MDI time series (left) and the shorter time interval of the IVM data (right). It is clear that, for this region, comparatively little energy is injected during the few hours immediately prior to the flare at approximately 23 hr. However, over the course of the previous day, a factor of four more energy is introduced. Thus we conclude that, in terms of the energetics, it is likely necessary to follow the evolution of a region for more than a few hours.

There is at present no source of high cadence long duration time series of vector magnetic field observations available. The long time series are needed to fully track the build up of magnetic free energy, and particularly for long time series, vector observations are important to separate out real evolution of the solar magnetic field from evolution resulting from projections effects inherent to line of sight observations. Thus the final results of our work effort were severely impacted by the denial of our request for a no cost extension to our contract. Our original proposal included applying the MCC model to data from the Solar Dynamics Observatory (SDO), but delays to launch of SDO mean they are still unavailable.

Evolution of Magnetic Properties for Two Active Regions

Although it is difficult to make reasonable energy estimates from the evolution of line of sight magnetograms, we have applied the MCC model to two active regions observed by the Hinode X-ray Telescope (XRT) and the Transition Region and Coronal Explorer (TRACE). One active region shows constant brightness in both XRT and TRACE observations. The other active region shows a brightening in the TRACE observation just after a decrease in X-ray brightness indicating the cooling of a coronal loop (see Fig. 3). By considering the *difference* in the behavior of the two regions in the MCC model (see Fig. 4), as applied to MDI line of sight magnetograms, we hope to learn more about changes in coronal energy release. This work is still proceeding under other sources of funding. An initial investigation based on the difference

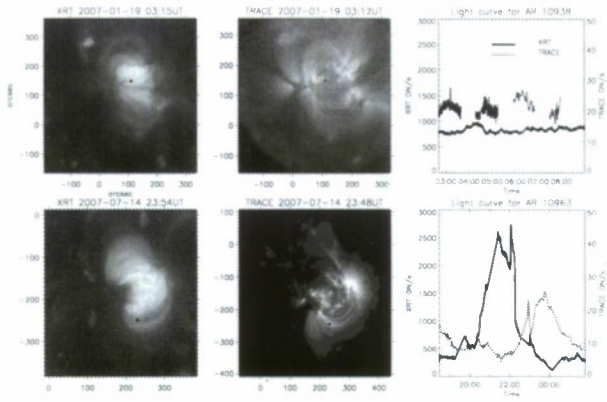

Figure 3: The small boxes near $(100'' \times 150'')$ on top and $(230'' \times -250'')$ on bottom represent the selected area of the light curve for AR 10938 and AR 10963, respectively. Solid and dotted lines represent the light curves for XRT and TRACE, respectively. [Adapted from Lee et al. (2009).]

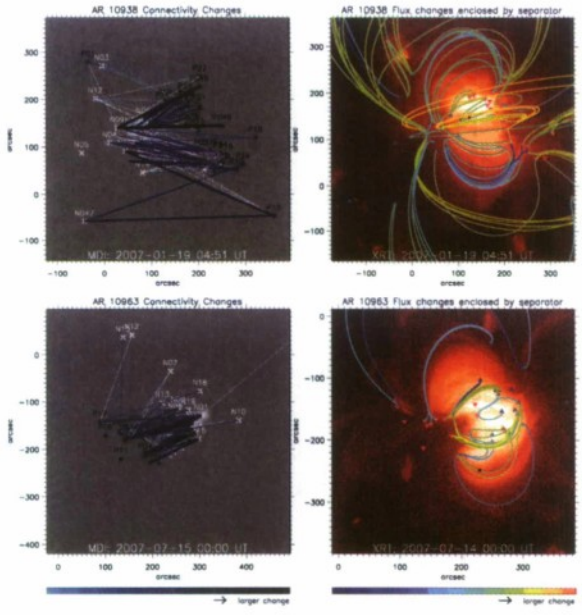

Figure 4: Left: MDI magnetogram with connectivity changes (lines) and point sources (+,× labeled by numbers). Thicker and darker lines show larger connectivity changes. Right: Changes in the flux enclosed by separators. Triangles represent nulls - positive (red), negative (blue), upright (moss green, near $180'' \times 180''$ on top), and coronal (green, near $270'' \times -190''$ on bottom). Black small boxes represent the location for light curve in Fig. 1. Yellow and orange lines represent larger flux changes. The same scales were used for two active regions. [Adapted from Lee et al. (2009).]

between two MDI images showed little difference between the two, as would be expected since the time interval is too short. Presently we are considering an approximately one day time interval, to see whether significant differences are found in the MCC model.

Helicity Decomposition

Using the partitioning algorithm developed for use with long time series of magnetograms,

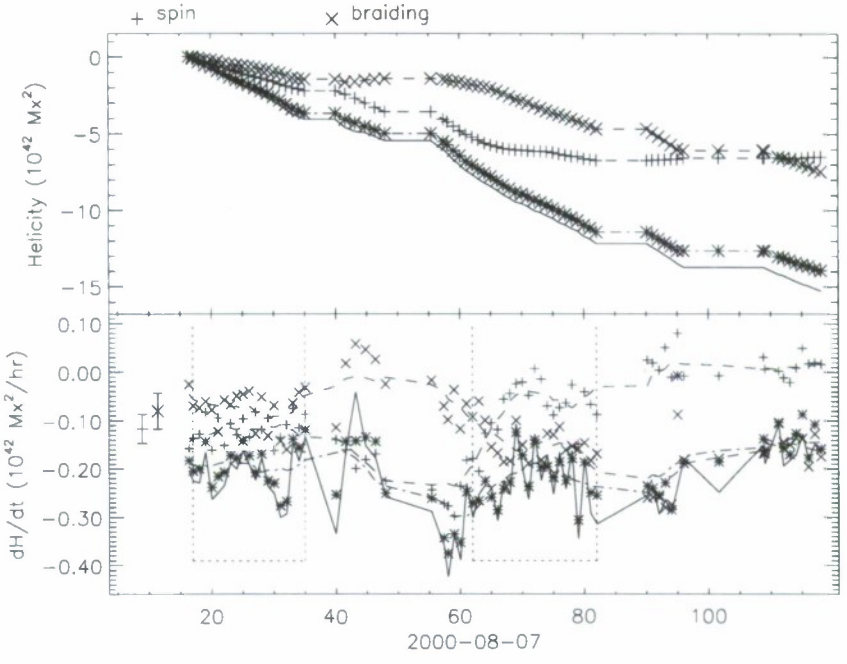

Figure 5: Summary of the helicity flux (bottom) and its integral (top) into NOAA AR 9114 plotted versus time in hours from 00:00UT on Aug-07. The total is indicated by a solid line, its decomposition into spin and braiding components is indicated by + and × respectively, and the sum of these is shown as a ∗. In this case, the rates of injection of spin and braiding helicity are comparable. [Adapted from Longcope, Ravindra & Barnes (2007).]

---

we have developed a method to usefully decompose the helicity flux across the photosphere into contributions of differing origin, called *spin* helicity and *braiding* helicity. These contributions would typically come at the expense of twist and writhe helicity, respectively, of a sub-photospheric flux tube anchored to the regions. The spin helicity of a given partition quantifies the mean rotation rate of motions internal to that partition, while braiding helicity is injected by the motions of whole partitions about one another. This decomposition is shown for NOAA AR 9114 in Figure 5. In this case, the contributions from the spin and braiding helicity are comparable.

Applying the method to six active regions shows cases where either spin or braiding dominates, and where they have the same signs and opposite signs. Thus it would seem that no general statement can be made regarding the dominance of twist or writhe in supplying helicity to the corona.

Connectivity Comparison

To determine the effects of the boundary conditions on the potential field connectivity, we studied in detail one active region: NOAA AR 8636 (Figure 6). The active region magnetic field was partitioned using the algorithm described in Barnes, Longcope & Leka (2005), to determine flux concentrations. The partitioning was repeated for a wide range of parameters, resulting in a range in the number of sources, from a few dozen in the coarsest partitioning, to a few hundred in the finest. For each way of partitioning the boundary, the connectivity

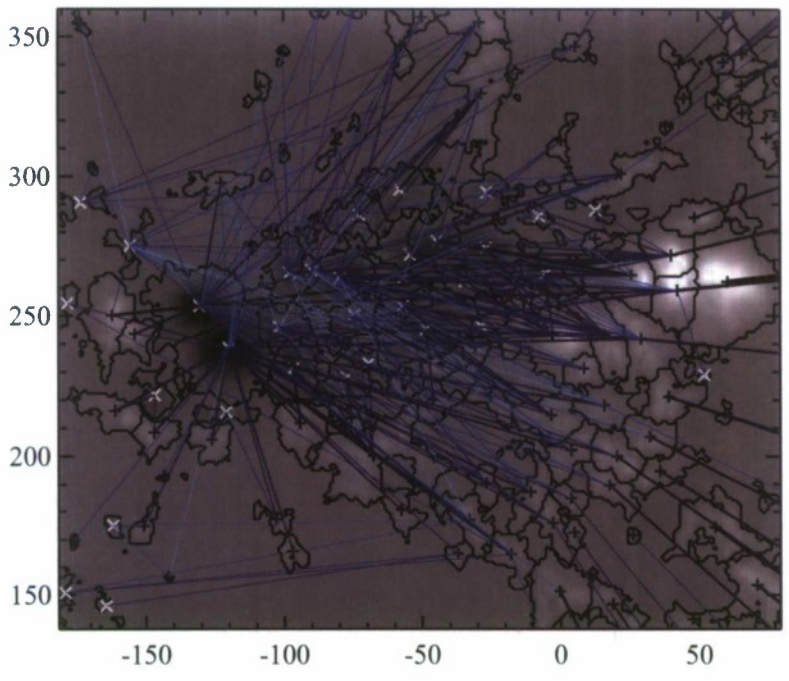

Figure 6: Connectivity for NOAA AR 8636. The vertical magnetic field is shown on a greyscale, sources are shown as $+,\times$ for positive and negative polarity, and the flux in each connection determines the thickness and color of the line segment connecting the sources, with large flux connections shown by dark, thick lines. This case has $N = 116$ sources.

---

was calculated in four ways: using the full magnetogram as a boundary condition (M) versus using point sources on the lower boundary (P), and letting the field fill the full half-space $z > 0$ (H) versus bounding the field with conducting walls outside the field of view of the magnetogram (B). For one set of partitioning parameters, a comparison of the MB and PB cases is shown in Figure 7 (left). For large flux connections, meaning those with more than about 10^{-3} of the total flux in the active region, there is relatively little difference between the two cases; for small flux connections, the difference can be large, with some small connections being completely absent in one case or the other. Overall, there is good agreement between the connectivities, with an overall flux discrepancy of 6.8% for this case. That is, over 90% of the flux in the region connects the same pairs of partitions in both ways of calculating the potential field.

This result of the large flux connections matching well, and the small flux connections having larger differences is a general property of the cases we considered. In Figure 7 (right), we show how the overall flux discrepancy changes as the partitioning is made finer, as represented by the number of sources. We found that the use of point sources makes a relatively small difference (5-7%) in the field connectivity, and that the greatest differences were in connections which contain relatively little flux, and thus are likely to be unimportant in the energetics of the region. Further, we found that changing the side boundary condition typically results in a larger (5-15%) difference in the connectivity. Thus the assumption made by the MCC model appears valid to within approximately 6%, and is not the dominant source of variations.

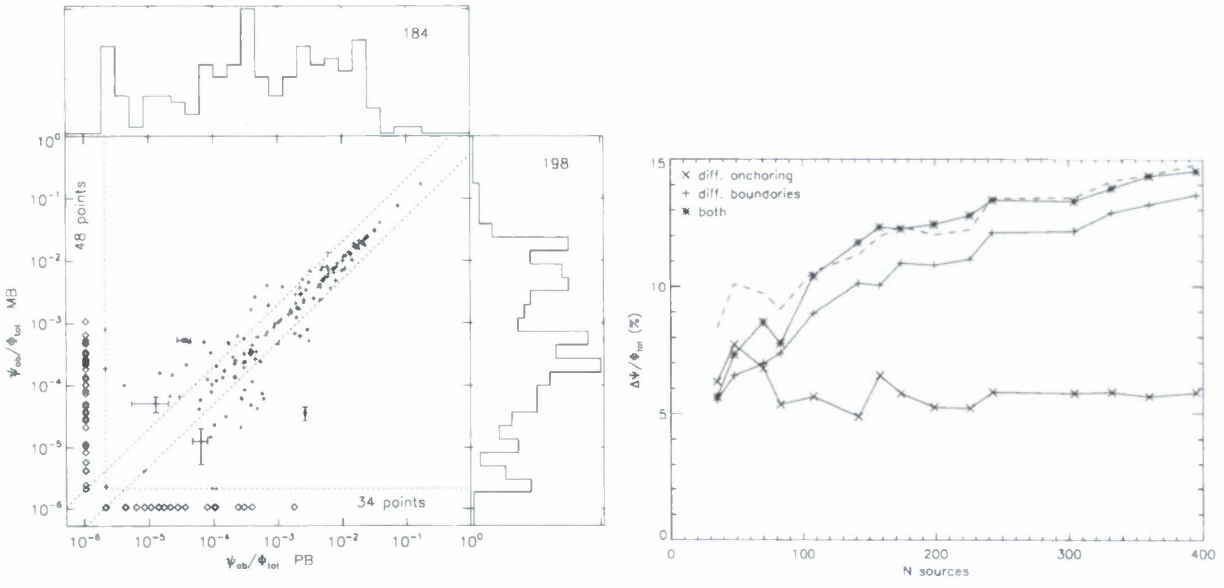

Figure 7: **Left:** The fluxes of identical connections from two different fields, MB (vertical axis) and PB (horizontal axis) plotted against one another. Fluxes are normalized to the total $\Phi_{\rm tot}$. Vertical and horizontal dotted lines show the minimum flux, ϕ_0. Singlet connections (absent from one of the fields) appear as diamonds below or to the left of these limits. For example, the vertical line of diamonds are absent from PB but present in MB with fluxes indicated by their position. The diagonal dotted lines mark $\psi_{ab}^{(MB)} = 2\psi_{ab}^{(PB)}$ (upper) and $\psi_{ab}^{(MB)} = \psi_{ab}^{(PB)}/2$ (lower). Statistical errors are indicated on a few representative points. Plotted along the right and top are histograms of $\ln \psi_{ab}$ for that field. The number appearing in the histogram gives the total number of connections. **Right:** The total connectivity difference, $\Delta\Psi_{X-Y}$, for different fields and different partitions. Comparisons are between fields with different anchoring $(MB - PB)$ ×, different boundaries $(PH - PB)$ +, and differing in both $(MB - PH)$ asterisks. All differences are plotted as a percentage of $\Phi_{\rm tot}$. The dashed lines shows $(\Delta\Psi^2_{MB-PB} + \Delta\Psi^2_{PH-PB})^{1/2}$ for comparison. If the changes in the connectivity from the anchoring and the boundaries were independent, one would expect the dashed line to match the asterisks, which is a reasonable approximation for most of the range shown. [Adapted from Longcope, Barnes & Beveridge (2009).]

Comparison of Flare Forecasting Parameters

In recent years, the number of parameters which have been proposed as potentially useful for flare forecasting has proliferated. One recently proposed parameter characterizes the "effective connected magnetic field", $B_{\rm eff}$, and has been described as "an efficient flare-forecasting criterion" (Georgoulis & Rust, 2007). To test this claim, we computed not just this parameter, but several other flare forecasting parameters which have previously been considered, for the same data base of active region magnetic field observations. The performance of each of these parameters was evaluated using a discriminant analysis approach developed for flare forecasting (Leka & Barnes, 2003; Barnes et al. 2007), as well as the all-clear forecasting approach described in Georgoulis & Rust (2007).

The following parameters were use for the comparison:

$\Phi_{\rm tot} = \int |B_z|$ - the total unsigned magnetic flux, often viewed as a standard for judging other

Table 1: Success rates and skill scores for the sample parameters.

parameter	success rate	skill score (binary)	skill score (probability)
climatology	0.908	0.000	0.000
$\Phi_{\rm tot}$	0.922	0.153	0.197
E_e	0.916	0.081	0.231
R	0.922	0.144	0.242
$B_{\rm eff}$	0.913	0.072	0.220

parameters.

$E_e = \int (\boldsymbol{B}^p - \boldsymbol{B})^2/8\pi$ - a proxy for the magnetic free energy (Leka & Barnes, 2003).

$R = \int_{HGPL} |B_l|$ - the total unsigned line-of-sight field close to high-gradient polarity-separation lines (Schrijver, 2007).

$B_{\rm eff} = \sum \psi_{ij}/|\boldsymbol{x}_i - \boldsymbol{x}_j|^2$ - the total of the flux connecting sources divided by the square of the distance between sources in an MCT model (Georgoulis & Rust, 2007).

The probability density of each of these parameters for a collection of over 1200 magnetograms is shown in Figure 8. In each case, there is a tendency for large flares to originate in regions with a large parameter value, but there is a great deal of overlap between regions which produce flares within 24 hr and those which do not.

To quantify this behavior, three measures of success are used, as shown in Table 1. For discriminant analysis, a binary prediction is made for each point, and the success rate - the fraction of regions classified correctly - is used. Although the success rates look impressively high, it is important to keep in mind that one can obtain a success rate of over 90% by predicting that all active regions will remain flare-quiet (first row of table). The *improvement* over this success rate for all of the parameters is modest at best.

The discriminant analysis approach has also been modified to produce probability forecasts, and the climatological skill score is used to judge their performance. The skill score measures the improvement over a uniform probability forecast, with a skill score of 1 for perfect forecasts, a skill score of 0 for no improvement over always predicting the same probability, and a negative score for worse performance. Again, the skill scores are not dramatically higher than zero, consistent with the modest improvements seen in the success rate.

We found that the parameter, $B_{\rm eff}$, proposed by Georgoulis & Rust (2007) does not perform significantly better than a similar parameter, $\phi_{\rm tot}$ considered by the PI and Co-I in a previous investigation supported by AFOSR. Indeed, when using discriminant analysis to estimate the success rate in forecasting the occurrence of major flares, it performs no better than parameters which characterize the photospheric magnetic field, but requires the additional step of computing the coronal magnetic topology. The coronal parameters may perform better for making "all-clear" forecasts, by predicting that regions with a parameter value smaller than the smallest observed to produce a flare will remain flare-quiet. This approach is very sensitive to a single measurement, and still only successful in correctly predicting an all-clear forecast for a small fraction of the possible all-clear intervals. Thus we feel that pursuing the MCC approach is likely to result in better forecasting results.

New and Refined Algorithms.

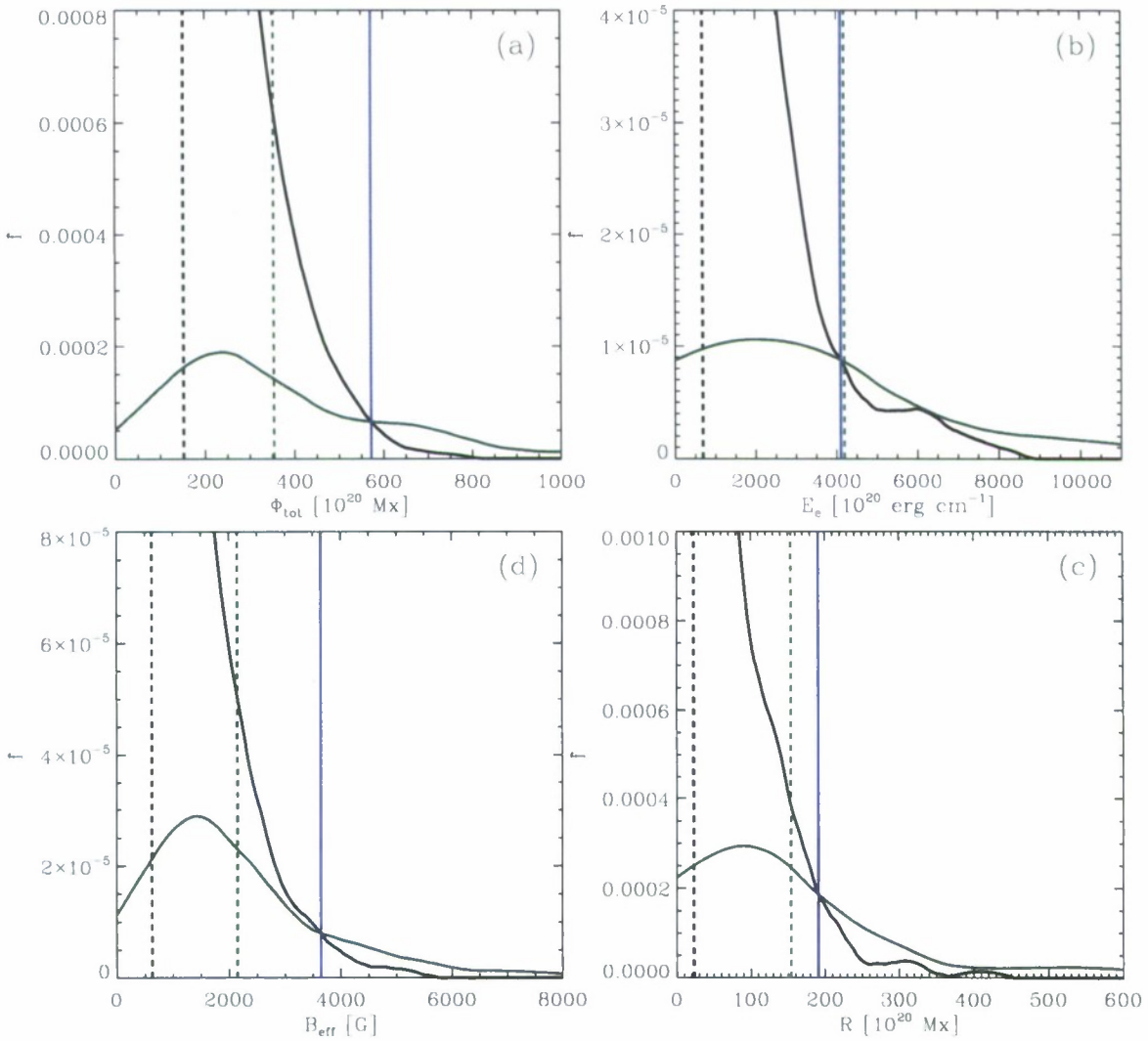

Figure 8: Nonparametric density estimates for the flaring (green) and nonflaring (black) populations for $\Phi_{\rm tot}$ (a), E_e (b), R (c), and $B_{\rm eff}$ (d). The discriminant boundary (50% probability forecast) is shown as a vertical blue line, and the sample means are shown as black/green vertical dashed lines. All the parameters exhibit similar behavior, with a tendency for regions with large parameter values to be more likely to produce an event, but no clear separation between the populations. [Adapted from Barnes & Leka (2008).]

Magnetogram Partitioning

A critical step in applying the MCC model is partitioning the active region field into distinct flux concentrations. To be useful in characterizing active region evolution, it is necessary to track the evolution of these flux concentrations over a long time interval, preferably of order days. The approach we have developed builds on a gradient based tessellation scheme: one partition consists of all pixels which are strictly downhill from a local maximum.

This scheme works well on any single magnetogram, but when applied to a time series, it can lead to large variations in the partitioning from one time step to the next. In particular,

it is frequently the case that a partition assigned to a single maximum at one time will, at the next time, contain two local maxima splitting the partition into two. To mitigate effects such as this, we use an approach, similar to Barnes, Longcope & Leka (2005), of adjusting each partition to minimize its differences with a reference. Barnes, Longcope & Leka (2005) constructed a reference by averaging an approximately hour-long time series of magnetograms with a cadence of a few minutes. For the much longer time series that may be needed to apply the MCC model, that approach will no longer work because of the significant evolution of the photospheric field.

Instead of a time-averaged reference for the entire time series, our new method constructs a new reference for each magnetogram by advecting, with the Local Correlation Tracking (LCT) velocity field, the partition from a neighboring time step. For the example presented here (see Figure 9), which contains regions of rapid flux emergence, it was preferable to start with the last time step, and advect the partitions backwards in time. Instances where a new source region appears will seem, in the reversed time, to represent the disappearance of an existing, labeled partition.

For the initial time the field is first smoothed by performing a potential-field extrapolation to a height of 1 pixel. This reduces the number of local maxima in $|B_{los}|$ resulting from noise. The gradient based tessellation scheme is then applied to assign a label to each pixel with a field strength exceeding 50 G.

This results in such a large number of partitions (typically several hundred) in regions of plage as to be unwieldy for subsequent calculations. To simplify the plage while maintaining the structure in sunspots, a saddle point merging is applied. That is, the field is evaluated at the saddle point between adjacent partitions, and if it is within 300 G of either maxima of the two partitions, the smaller flux partition is assigned the same label as the larger flux partition. With this criterion, the plage is simplified to a tractable number of sources (generally less than 100). Our hope in this approach is that the important effects in the corona for solar flares and CMEs are rooted in regions of strong field, so the exact representation of weak fields is not crucial.

In order to validate the partitioning, a comparison has been made between the centroid velocity and the flux-weighted average of the LCT velocity for each partition. If the partitioning algorithm is consistently tracking the same photospheric flux, these velocities should be the same. Figure 9 shows the results of this comparison for NOAA AR 9114. This region was chosen because the velocity of its central sunspot was also the subject of analysis by Brown et al. (2001), so that additional comparisons could be made. Both qualitatively and quantitatively, there is good agreement between the two methods for determining the velocity. Thus we are confident that the partitioning is indeed following concentrations of photospheric flux as an active region evolves.

Null Finding Procedure

The null finding algorithm begins by sorting sources into ascending (descending) order for regions with a net negative (positive) flux. Neglecting all other sources, the null point associated with the first two sources is determined analytically. Each additional source is then reintroduced, initially with a flux 10^{-3} smaller than its actual value. The new null point thus introduced is located from an initial guess given by considering the new source plus a uniform field equal to the field due to all the other sources at the location of the new source. This initial guess for the null location is refined using a globally convergent multi-dimensional Newton-

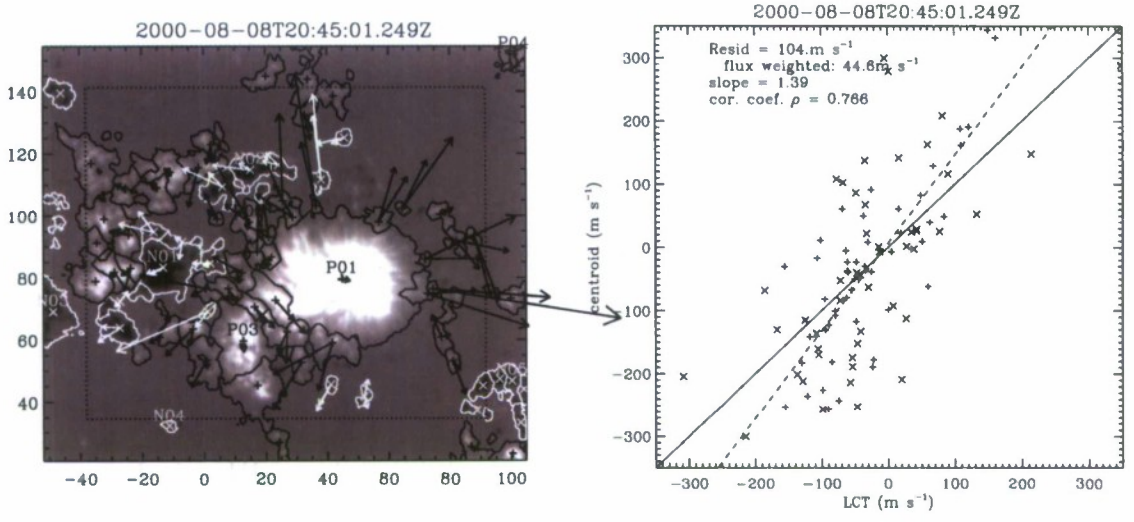

Figure 9: Comparison of the centroid and LCT velocities for NOAA AR 9114. **Left:** A high resolution MDI magnetogram, with axes labeled in arc-seconds from disk center. The dotted line bounds the region in which the LCT velocity is determined. For partitions entirely within this region, the velocities as determined by both LCT and fitting the location of the centroid are shown as arrows, with length proportional to the speed. There is qualitatively good agreement in the magnitude and direction of the velocity. **Right:** The centroid velocity, $d\bar{\boldsymbol{x}}_a/dt$, *vs* the flux-weighted average of the LCT velocity at each pixel, $\bar{\boldsymbol{u}}_a$. The x-component of the each velocity is shown with a $+$; the y-component is shown with a $\times$. The dashed line is the regression line. The correlation coefficient is $\rho = 0.77$, indicating good agreement between the methods. [Adapted from Longcope, Ravindra & Barnes (2007).]

Raphson root finding algorithm. The charge on the new source is then slowly ramped up to its final value, and the location of each null point is updated by using its previous location as an initial guess for the Newton-Raphson algorithm.

At each increment in the magnitude of the source charge, checks are made for local separator bifurcations and for pitchfork bifurcations both of which result in the creation of two new null points. This procedure is likely to fail when more than one bifurcation occurs during a single incrementing of the source charge. To guard against this behavior, while also maintaining a reasonable speed for the algorithm, once each source has been fully reintroduced, the Euler characteristics given in Longcope & Klapper (2002) are checked. If they are not satisfied, then the source is turned off and reintroduced more slowly until the Euler characteristics are satisfied.

Technical Feasibility:

At this stage, it is difficult to judge the technical feasibility of this approach to predicting flare properties. We have determined that applying the MCC model to short time series of vector magnetograms does not recover the energy build up, but this is almost certainly because the process of building up energy occurs on a time scale of days. We have developed most of the necessary tools to apply the MCC model to longer time series, but an appropriate source of data is not presently available, although we anticipate that the HMI instrument on

SDO will provide such data in the near future, with a launch data presently schedule for 2009 November. Until these data are analyzed, it is impossible to judge how well the model will work. Nevertheless, the code which has thus far been developed is capable of running in real time, making it a potentially useful prediction tool.

Personnel Supported:

Graham Barnes and K.D. Leka were supported by this contract. In addition, the research effort was performed in association with Dana Longcope, Colin Beveridge and B. Ravindra, at Montana State University, and J.-Y. Lee, at Harvard-Smithsonian Center for Astrophysics and NorthWest Research Associates.

Publications:

J.-Y. Lee, K.D. Leka, G. Barnes, K.K. Reeves, K.E. Korreck and L. Golub, 2009: "Evolution of magnetic properties for two active regions observed by Hinode/XRT and TRACE", Proceedings of the GONG 2008/SOHO 21 Meeting, submitted.

D.W. Longcope, G. Barnes and C. Beveridge, 2009: "Effects of Partitioning and Extrapolation on the Connectivity of Potential Magnetic Fields", *Astrophys. J.*, **693**, 97-111.

G. Barnes and K.D. Leka, 2008: "A Comment on 'Quantitative Forecasting of Major Solar Flares"', *Astrophys. J.*, **688**, L107–L110.

D.W. Longcope, B. Ravindra and G. Barnes, 2007: "Determining the Source of Coronal Helicity Through Measurements of Braiding and Spin Helicity Fluxes in Active Regions", *Astrophys. J.*, **668**, 571–585.

Interactions/Transitions:

Preliminary results of the work were presented as follows:

"Magnetic Charge Topology Analysis for Space Weather Forecasting" – G. Barnes and K.D. Leka, poster at the 2008 fall AGU meeting.

"Forecasting of Solar Flares From Vector Magnetogram Data" – G. Barnes, invited talk at the 2008 Space Weather Workshop.

"A Comparison of Solar Flare Forecasting Methods" – G. Barnes, invited talk at NOAA's Space Weather Prediction Center.

"A Comparison of Selected Flare Forecasting Parameters" – G. Barnes and K.D. Leka, contributed talk at the 2007 Living With a Star meeting.

"A Comparison of Flare Forecasting Parameters Derived From Photospheric Magnetograms" – G. Barnes and K.D. Leka, poster at the 2007 fall AGU meeting.

"A Comparison of the Topology of Potential Magnetic Fields Inferred for Solar Active Regions" – G. Barnes, C. Beveridge, D.W. Longcope and K.D. Leka, poster at the 2007 SHINE workshop.

"Estimating Active Region Free Energy from the Minimum Current Corona Model" – G. Barnes, C. Beveridge, D.W. Longcope, B. Ravindra, K.D. Leka at the 26^{th} General Assembly of the International Astronomical Union.

"A Free Energy Estimate from the Minimum Current Corona Model" – G. Barnes, C. Beveridge, D.W. Longcope, B. Ravindra, K.D. Leka at the 2006 SHINE workshop.